Cascade overlap and amorphization in 3C-SiC: Defect accumulation, topological features, and disordering

F. Gao* and W. J. Weber
Pacific Northwest National Laboratory, MS K8-93, P.O. Box 999, Richland, Washington 99352
(Received 17 December 2001; revised manuscript received 12 March 2002; published 3 July 2002)

Molecular dynamics (MD) simulations with a modified Tersoff potential have been used to investigate cascade overlap, damage accumulation, and amorphization processes in 3C-SiC over dose levels comparable to experimental conditions. A large number of 10 keV displacement cascades were randomly generated in a model crystal to produce damage and cause amorphization. At low dose, the damage state is dominated by point defects and small clusters, where their concentration increases sigmoidally with increasing dose. The coalescence and growth of clusters at intermediate and higher doses is an important mechanism leading to amorphization in SiC. The homogeneous nucleation of small clusters at low dose underpins the homogeneouslike amorphization observed in SiC. A large increase in the number of antisite defects at higher dose indicates that both interstitials and antisite defects play an important role in producing high-energy states that lead to amorphization in SiC. The topologies (such as total pair correlation function, bond-angle, and bond-length distributions) of damage accumulation in the crystal suggest that a crystalline-to-amorphous (*c-a*) transition occurs at about 0.28 dpa. This value is in qualitative agreement with the experimental value of 0.27 dpa under similar irradiation conditions. After the model crystal transforms to the fully amorphous state, the long-range order is completely lost, while the short-range order parameter saturates at a value of about 0.49.

DOI: 10.1103/PhysRevB.66.024106 PACS number(s): 61.80.−x, 61.72.Ji, 61.82.Fk, 71.15.Pd

I. INTRODUCTION

Silicon carbide (SiC) has a number of outstanding physical and chemical properties that drive its potential application in semiconductor devices, high neutron radiation environments, and in the petrochemical industries.[1] The high-electron mobility, wide band gap, high-breakdown field, and high saturated electron-drift velocity make SiC suitable for high-power and high-frequency electronic device applications.[2] The small cross section, low activation and good thermal conductivity under neutron irradiation lead to its potential use in structural components for fusion reactors,[3] as an inert matrix for the burnup of plutonium from excess weapons,[4] and as cladding material for gas-cooled fission reactors.[5] In device processing, ion implantation is an important technology for donor or acceptor doping, but this process results in the creation of atomic-level defects whose accumulation can cause disordering and amorphization. Investigation of the production and subsequent evolution of nonequilibrium concentration of defects in SiC is thus of considerable technological, as well as scientific, interest. In spite of the technological importance of SiC, damage formation, defect accumulation, and disordering are not well understood, particularly with regards to the atomic-level mechanisms controlling the crystalline-to-amorphization (*c-a*) transition. The loss of crystallinity or amorphization in SiC has been the subject of numerous experimental studies over the last decades. The comprehensive reviews of the extensive experimental[6–8] and theoretical[9] efforts appear in the literature. Despite these efforts, the study of the mechanisms leading to the *c-a* transition in SiC remains an important challenge that demands atomic-level insight of the dynamic processes controlling the evolution of irradiation damage and defect accumulation that can be provided by MD simulations.

Using a range of analytical techniques, the irradiation-induced crystalline-to-amorphous transformation in SiC has been studied as a function of temperature under irradiation with electrons,[10,11] neutrons,[12] and various ions.[13,14] The *c-a* transition occurs below a critical temperature only after a critical defect concentration is exceeded. The critical energies and threshold doses for complete amorphization in SiC for a given irradiation condition have been determined as a function of temperature. It is generally accepted that homogeneouslike amorphization in SiC is the dominant process, even under heavy-ion irradiation, which may be associated with the accumulation of irradiation-induced defects, nanoscale amorphous nuclei, and the overlap of damage cascades.

Molecular dynamics (MD) simulations have long been used to study the nature of the primary damage state produced by fast atomic particles in metals[15,16] and ceramics.[17,18] Several computational studies have been recently performed to investigate the displacement threshold energies and single displacement cascades with energies up to 50 keV in 3C-SiC using variations of the Tersoff potentials.[17,19–21] These studies have provided much insight into the mechanisms that control defect production in displacement cascades and statistics on the nature and number of defects generated as a function of energy. The results show that self-atom recoils in SiC lead to the formation of dispersed cascades, where the defects are spread over the simulation cell, as illustrated in Fig. 1(a).[21] Most surviving defects are single interstitials and vacancies, such that only 19% of the interstitial population is contained in clusters. The size of the defect clusters is small, and defect clusters containing more than four defects are seldom produced within a single cascade, as shown in Fig. 1(b).[21] These results suggest that in-cascade or direct-impact amorphization in SiC does not occur with any high degree of probability during the cascade lifetime, even with high-energy recoils.[21]

 ©2002 The American Physical Society

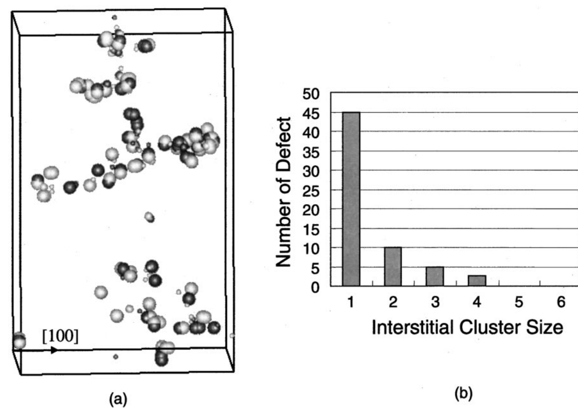

FIG. 1. (a) Atomic plot of defects produced by a 10 keV Si cascade, where defect type is distinguished by size and gray shading and (b) the distribution of interstitials clusters per cascade for Si recoils in SiC at 300 K.

Although there are experimental techniques, such as high-resolution transmission electron microscopy, currently applied to study the dynamics of amorphization processes, it remains unclear why homogeneouslike amorphization is the dominant process in SiC, even under heavy-ion irradiation. In contrast, heterogeneous amorphization appears to occur in a majority of ceramics.[22] Therefore, it is necessary to simulate cascade overlap to determine how defects and defect clusters accumulate and how amorphous domains nucleate and grow into large amorphous regions during such processes.

Previously, Malerba *et al.*[23] employed molecular dynamics to simulate defect accumulation with 100 eV recoils in SiC. Their results suggested that the driving force for the crystalline-to-amorphous (*c-a*) transition under these conditions is the accumulation of Frenkel pairs. Antisite defects, which are not readily produced by 100 eV recoils, but are produced in large numbers at higher energies,[24] apparently do not play a significant role under these low-energy conditions. Major changes in SiC under these simulation conditions take place because of the increase in Frenkel pairs. The eventual production of antisite defects from collision processes scarcely influences the energetics of the system. Since the recoil energy of 100 eV is well below that necessary to define a real cascade process, the conditions of the Malerba *et al.*[23] simulations correspond to electron irradiation. Their simulation results are in reasonable agreement with experimental electron-irradiation results.[10,11] More energetic displacement cascades produce not only Frenkel pairs and antisite defects, but also clusters.[20,21,24] Recent experimental results[6] have shown that many small clusters are produced throughout the irradiation region in SiC irradiated with Fe^{2+} ions at low dose (0.08 dpa at damage peak). A partially amorphous state is observed in regions irradiated to a dose greater than 0.2 dpa. Furthermore, a completely amorphous state was attained at a higher dose of 0.4 dpa at the surface. However, the nature and microscopic role of these clusters in the nucleation and growth of amorphous domains is still not fully understood. Atomic-level simulations to interpret experimental results are required to explore the mechanisms controlling *c-a* transition, and to develop models of radiation-induced structure-property changes.

In this paper, a molecular dynamics (MD) method has been employed to simulate defect accumulation, cascade overlap and disordering in 3C-SiC, and the dynamic processes are followed from a low dose level to complete amorphization. This paper describes the model and method employed in the present simulations, and the results for defect accumulation; the following paper (Ref. 25) deals with the energetics of the system, radiation-induced volume changes due to defect accumulation and amorphization, relative disorder of Si and C atoms, and TEM images of damage accumulation. In the following, the evolution of cascade overlap, the accumulation of interstitials, vacancies and antisite defects are presented in Sec. III. The *c-a* transition during cascade overlap and the topological features of amorphous state, such as coordination number, pair correlation function, bond length and bond angle, are described in Sec. IV, followed by the calculations of ordered parameters as a function of dose in Sec. V. Discussion and comparison with experimental results and those obtained by others will be given in Sec. VI.

II. SIMULATION DETAILS

The MD simulations of cascade overlap were performed using a parallel version of MDCASK code, which has been modified to study SiC,[17] with constant pressure and periodical boundary conditions. The number of atoms contained in the simulation cell was kept constant, while the temperature is controlled by coupling the atoms in the two boundary planes along the z direction to a reservoir of heat at 200 K. The shape of the MD block is rectangular and contains $10\times10\times50$ unit cells with 40 000 atoms.

The energy of 10 keV was chosen for the cascade energy in the present simulation study because higher-energy cascade simulation (up to 50 keV) yields multiple branches with energies on the order of 10 keV.[20] Selection of this energy allows the use of a smaller MD block, which makes the simulation tractable computationally. The energy of 10 keV for the Si recoil is also near the peak in the nuclear stopping power for Si in SiC, which according to the stopping and range of ions in matter (SRIM) code[26] occurs at 12 keV; thus, the simulations will investigate the regime of highest-energy deposition density. Since many experimental studies follow the accumulation of damage at the peak in the damage production profile (i.e., damage peak), the present simulation study is directly relevant to previous experiments, such as those employing Si or Ar ions where the energies of the incident ions and recoils in the damage peak are on the order of 10 keV.[9,13]

The simulation of cascade overlap processes in SiC was started by giving an atom near the top of the cell a kinetic energy of 10 keV into the cell, which generated an initial 10 keV displacement cascade. The displacement cascade was allowed to evolve for about 10 ps, after which the MD cell was equilibrated for another 10 ps to control temperature. Creating a second cascade simulated cascade overlap, and the production of subsequent cascades with a similar procedure, except with random atoms and directions, provided a

simulation of multiple cascade overlap. Each subsequent cascade was allowed to evolve for at least 10 ps, such that the collisional and thermal spike stages of the cascade could be assessed, and the MD cell was again thermally equilibrated for 10 ps. A Wigner-Seitz cell method has been used to identify interstitials, vacancies and antisite defects. A lattice site with an empty Wigner-Seitz cell was recognized as a vacancy, a cell with multiple atoms is an interstitial and a site occupied by a wrong atom type is designated as an antisite defect. Currently, additional analysis efforts are underway to compare the ratio of interstitials to antisite defects in SiC for different criteria, such as nearest-neighbor spheres and Lindemann spheres, and an analysis of damage accumulation based on topological considerations is being performed.

After each overlap event, the damage state and the energy of system were stored for subsequent analysis, and the corresponding dose level was calculated. Relative disordering, the topological distribution and ordered parameters were sampled every five cascades, averaging over 5000 time steps. After each cascade, an accounting of defects was performed, and the corresponding dose was determined based on the average number of displaced atoms produced by a 10 keV Si cascade in 3C-SiC, which previous detailed MD experiments[17,21] in 3C-SiC have shown to be about 100 displacements, multiplied by the number of cascades, and divided by the total number of atoms in the MD block. Although this method may involve some degree of uncertainty, it is consistent with the methods applied to experimental data, where the average number of local displacements per ion, based on the SRIM code, is multiplied by ion flux and divided by the atomic density of virgin crystal. To distinguish the dose in these simulations from those in experimental studies, the unit of dose used is MD-dpa to avoid any confusion regarding the method of calculation. A total of 140 cascades were simulated, corresponding to a final dose of 0.35 MD-dpa. Frenkel pairs and antisite defects were globally accumulated over a time span of about 3 ns, which gives a dose rate on the order of 10^8 MD-dpa/s. This dose rate is significantly greater than any experimental value used. However, dose rate effects should only be important when there is significant mobility of the defects, which is generally not the situation during low-temperature irradiation of SiC. Therefore, the dose rate employed in the present simulations should reasonably mimic experimental defect accumulation and disordering processes at low temperatures.

The interactions between atoms were described using Tersoff potentials along with a modification of short-range interactions based on *ab initio* calculations,[17] where the cutoff distances of the potentials were scaled by the cell volume. The threshold displacement energies determined using these potentials are in good agreement with those obtained by first-principles calculations and experimental methods,[27] and the melting temperature simulated is in reasonable agreement with experimental value.[20] These potentials have also been employed to calculate defect properties[28] and displacement cascades for recoil energies from 0.25 to 50 keV in 3C-SiC.[24] These results suggest that the potentials are well suited for the present simulations of damage accumulation. In order to characterize the topologies of partial and complete amorphization irradiated in SiC, a reference amorphous sample has been prepared using the same Tersoff potentials. A crystal containing 1728 atoms was initially heated to 3900 K using a method called semiconstant volume simulation, as described by Gao and Weber,[20] and the melting process was observed at 45 ps. The crystal was further equilibrated for another 120 ps to allow proper atomic mixing, and then quenched to 0 K. Although this may not reproduce all the properties of amorphous SiC, it provides a simple method that is sufficient for evaluating the possible aspects of topological features.

III. CASCADE OVERLAP AND DEFECT ACCUMULATION

The present MD simulations have studied defect and damage accumulation from a single cascade, which represents the lowest damage state, to the completely amorphous state produced by multiple cascade overlap. Therefore, a full comparison with experiments can be made. Furthermore, the mechanisms and the exact nature associated with the amorphization processes in SiC are investigated. Figure 2 shows the damage states produced in the central part of the MD block as a function of equivalent dose, where only displaced atoms and antisite defects are plotted for simplicity. Large spheres represent the displaced atoms, while the antisite defects are indicated by small spheres. At low dose, the dominant defects are single interstitials and monovacancies, but it can be clearly seen that some small clusters are nucleated in Fig. 2(a), as indicated within the circle. The size of the clusters is very small, similar to those found in a single cascade.[20] However, the concentration of small clusters increases with increasing dose and these clusters are distributed randomly inside the MD block. These clusters are three-dimensional clusters of point defects, which should induce considerable strain in the lattice. A preliminary result of cascade annealing indicates that small clusters in SiC have low mobility, which should promote the formation of disordered states. During continued cascade overlap, the small clusters coalesce and grow, due to local strain, to form larger clusters or amorphous domains, which are surrounded by many small clusters, as illustrated in Figs. 2(b) and 2(c). Thus, the amorphization process appears to be consistent with the defect-stimulated cascade-induced growth of small clusters, discussed further in Sec. VI. A detailed analysis indicates that these larger amorphous domains consist of interstitials and antisite defects, as well as vacancies, suggesting that both interstitials and antisite defects play an important role in the high-energy states that lead to amorphization in SiC. It is observed that some small clusters containing only two or three defects are dissociated by direct collision from energetic recoils. The defects dissociated from the clusters annihilate, become isolated defects, or combine with other defects or clusters. The competition between nucleation and elimination of small clusters represents a dynamic process for cluster formation during cascade overlap. The increase in the number of clusters with increasing dose suggests that the nucleation of small clusters is a dominant process in SiC. The coalescence and growth of clusters gives rise to the formation of larger amorphous regions, as seen in Figs. 2(d) and

FIG. 2. (Color) Computer plots showing the process of cascade overlap and defect accumulation as a function of dose, the nucleation of small clusters and the coalescence of clusters, where only interstitials and antisite defects are presented. The legend identifies the four possible defect type: C interstitial (C^I), Si interstitial (Si^I), C sublattice antisite (Si_C), and Si sublattice antisite (C_{Si}).

2(e). A completely amorphous state is reached at a dose of about 0.28 MD-dpa, as shown in Fig. 2(f), where interstitials, vacancies and antisite defects are distributed homogeneously. Such homogeneouslike amorphization is associated with several possible processes during cascade overlap: (a) the production and accumulation of point defects and small clusters that act as amorphous nuclei at low dose; (b) the nucleation of additional small clusters due to local high defect concentration; and (c) the local growth and coalescence of clusters to form amorphous domains. The damage accumulation due to Si ions in 6H-SiC has been studied experimentally by ion implantation and *in situ* RBS measurements.[29,30] These results have shown that point defect production appears to dominate at a low dose level (<0.04 dpa in the damage peak region), which is supported by subsequent isochronal annealing over a temperature range from 190 to 1200 K; while at higher dose level, a buried amorphous layer is formed at a dose of 0.3 dpa.[30] The present simulations are qualitative agreement with the experimental observations, which supports the proposed mechanisms of defect-stimulated nucleation and growth of small clusters during continued cascade overlap.

To demonstrate the damage accumulation due to cascade overlap, the numbers of interstitials and antisite defects are shown in Fig. 3 as a function of dose, where the Si and C components are presented separately. In general, interstitials and antisite defects increase sigmoidally with increasing dose. The increase is slow at low dose level, which may reflect the accumulation of only point defects and the nucleation of small clusters, as discussed above. Cascade overlap results in increased defect production due to prior-existing

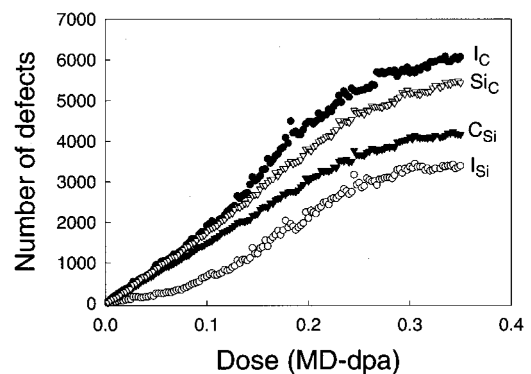

FIG. 3. Data for the number of interstitials and antisites defects as a function of dose in irradiated SiC, where the Si and C components are presented separately.

defects and the nucleation of clusters between existing clusters causing growth and coalescence. The enhanced defect production due to cascade overlap leads to a faster increase in interstitial production above a dose of 0.05 MD-dpa, and the increase is very small after 0.28 MD-dpa, which suggests the c-a transition has been achieved. It should be pointed out that the results in Fig. 3 are obtained using Wigner-Seitz-cell analysis that is based on original lattice sites, as described in the simulation details above. While this method may be inappropriate for addressing chemical and topological disorder, as suggested by Yuan and Hobbs,[31] particularly for the highly disordered, near-amorphous state. The Wigner-Seitz method is consistent with the method of determining defect concentrations and disorder using experimental ion-channeling methods, where all the displaced or disordered atoms are referenced to a perfect crystal structure that is also not present at high doses. Since one objective of this study is to make comparisons to experimental results, the Wigner-Seitz method provides an imperfect but consistent method with the experimental technique most often employed.[7,8,13,29,30,32] Other methods of analysis based on topological disorder cannot be directly compared to experimental results, because at present topological disorder does not provide the basis for any experimental method that can be easily employed with ion-beam irradiated samples.

Irradiation experiments have been performed at 190 K with 550 keV Si ions over range of fluences in 6H-SiC (Refs. 29,30) and at ~170 K with 360 keV Ar ions in both 6H-SiC (Ref. 30) and 3C-SiC.[13] It was found that the damage behaviors for 6H-SiC and 3C-SiC are almost identical. Conventional 2.0 MeV He^+ Rutherford backscattering spectrometry (RBS) in channeling geometry has been used to characterize the disorder on the Si sublattices. Based on these data, the results have shown that the full amorphization dose is on the order of 0.3 dpa for 6H-SiC irradiated at 190 K with 550 keV Si and 0.27 dpa (corrected for revised threshold displacement energies[27]) for 6H-SiC and 3C-SiC irradiated at ~170 K with 360 keV Ar. The value of 0.28 MD-dpa determined from the MD simulations is in qualitative agreement with these experimental data. Furthermore, it is clear that the number of C interstitials I_C is greater than that of Si interstitials I_{Si} for all doses simulated, which is consistent with the smaller threshold energy for C atoms in the SiC system[24] and with recent experimental results in 6H-SiC.[32] These interstitials represent the true number of defects, since the two displaced atoms that form a dumb-bell have been counted as one self-interstitial atom (SIA) and the empty lattice site at the center of a SIA dumbbell has been neglected in the count. The ratio of the number of C interstitials to Si interstitials R_{int} as a function of dose is plotted in Fig. 4, together with that of C antisites to Si antisites R_{ant}. At low dose, the interstitial ratio is, on average, about 3.8, which is in good agreement with those found in single cascades. Typical values of this ratio are 3.5 for 10 keV cascades[17] and 3.2 for 50 keV cascades.[20] The decrease of R_{int} with increasing dose is consistent with the formation or growth of large clusters or amorphous domains within which both Si and C atoms are collectively displaced into interstitial positions, as seen in Fig. 2. The saturation value of about 1.7 at a dose of 0.28 MD-dpa remains virtually unchanged up to higher dose levels, which suggests that the c-a transition is achieved. Unlike R_{int}, R_{ant} increases linearly with increasing dose, but the increase is very small. This plot, together with Fig. 3, clearly indicates that the number of C antisite defects Si_C is greater than that of Si antisite defects C_{Si}, as expected. A large numbers of antisite defects are produced during the cascade-overlap process, particularly at high dose where the total number of antisite defects is comparable with that of interstitials. For example, 9587 antisite defects are produced as compared with 9464 interstitials at 0.35 MD-dpa. This has clearly demonstrated that the driving force for the c-a transition is due to the accumulation of both interstitials and antisite defects, supporting a previous assumption that the generation of antisite defects may play an important role in the amorphization process in SiC.[33]

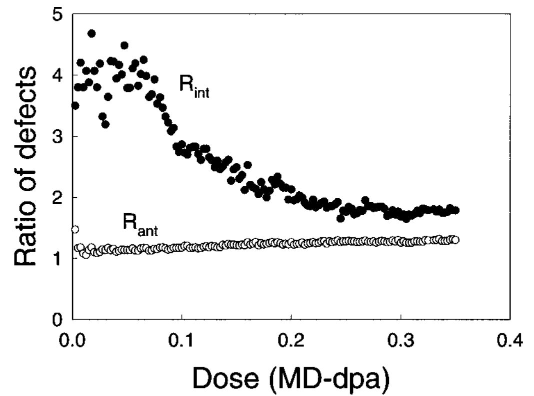

FIG. 4. The ratio of the number C interstitials to Si interstitials R_{int} as a function of dose, together with the ratio of the number of C sublattice antisites to Si sublattice antisites R_{ant}.

Atomic mixing indicates an important feature in ion-implantation-induced modification of materials and is a measure of the rearrangement of the atomic configuration. It is known that SiC has a very poor mixing efficiency, and much less rearrangement of atoms occurs during a single cascade process.[17] The value of the mixing parameter increases with damage energy from a value of about 0.5 at 250 eV to a saturation value of 2.3 at 5 keV, remaining virtually unchanged up to 50 keV.[24] Therefore, it is of interest to see how the atomic mixing varies with dose during cascade overlap. The mixing efficiency Q can be obtained from the mean square displacements of atoms and is given by

$$Q=\frac{\Sigma_{i=1}^{N}[r_i(t)-r_i(0)]^2}{6n_0E_p}, \tag{1}$$

where E_p is PKA energy, n_0 the atomic density, and $r_i(t)$ the atomic displacement at time t. The atomic mixing during cascade overlap is calculated and shown in Fig. 5 as a function of dose. The increase in atomic mixing with increasing dose is almost linear, and the larger mixing efficiency of C compared to Si atoms suggests that C atoms play a major role, and much more rearrangement of C atoms occurs during the cascade overlap process. Although the number of defects is almost saturated after the c-a transition, the mixing parameter still increases with increasing dose. This indicates

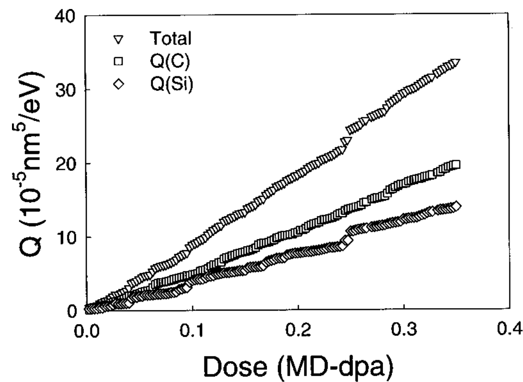

FIG. 5. The atomic mixing parameter calculated for 3C-SiC as a function of dose, where the contribution from Si and C atoms is plotted separately.

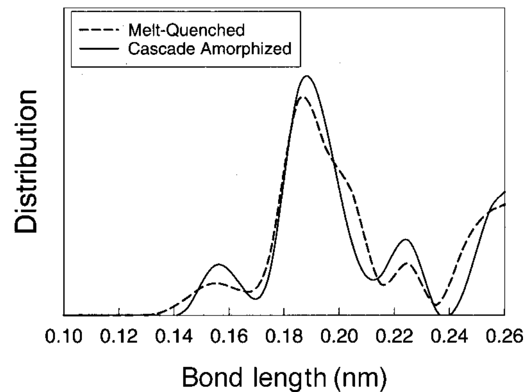

FIG. 7. Comparison between bond-length distribution functions for amorphous SiC at the end of cascade overlap and the reference melt-quenched sample.

that a large atomic rearrangement takes place without further increase in defect production. It is noted that there are some discontinuities in the Si atomic mixing efficiency, but not in the C mixing. Because of the larger displacement and mixing rate for C relative to Si, the observed discontinuities may be associated with Si mixing driven by a need to maintain or establish certain topological features, some of which may be artifacts of the interatomic potential. A detailed understanding of these discontinuities may come out of the ongoing topological analysis of the damage states.

IV. TOPOLOGICAL FEATURES OF AMORPHOUS SiC

The pair-correlation function of the MD cascade-amorphized (CA) SiC at the dose of 0.28 MD-dpa is shown in Fig. 6, together with those obtained from the MD melt-quenched (MQ) amorphous sample, where the contributions from Si-C, C-C, and Si-Si pairs are presented separately. In general, the pair-correlation function for CA-SiC is very similar to that of MQ-SiC sample, particularly in the positions and size of peaks, and their distributions show the typical systems without periodicity and liquidlike structure. The small peak of C-C pair appears at about 0.15 nm, which is comparable to the nearest-neighbor distance for graphite (0.143 nm) and diamond (0.155 nm) and believed to arise from C π binding. This peak represents C-C-C configurations. The second peak of C-C pairs is at about 0.308 nm, and corresponds to the different bonding of C-C pair with Si atoms, particularly forming C-C-Si configurations in SiC. It can be also seen that there exists a small shoulder on the C-C pair at 0.25 nm between the first and second peak on the C-C pair, which is very close to the next-nearest-neighbor distance of diamond (0.249 nm) and is related to the formation of diamondlike structures of carbon atoms in the CA-SiC. These different bonds formed by C-C pairs represent planar (sp^2) and tetrahedral (sp^3) carbon-binding microstructures that have been observed experimentally[34] and indicated by *ab initio* calculations in an amorphous SiC.[35] The maximum of the Si-C bonding appears at 0.189 nm and corresponds to the nearest-neighbor distance of 3C-SiC, which may describe C-Si-C or Si-C-Si configurations. The three curves have a pronounced peak near 0.3 nm, corresponding to different bonding arrangement of the two species, particularly to Si-Si-C and Si-C-Si configurations. These, along with sp^2 and sp^3 carbon-binding structures, give a rather complicated picture of the CA-SiC and MQ-SiC samples.

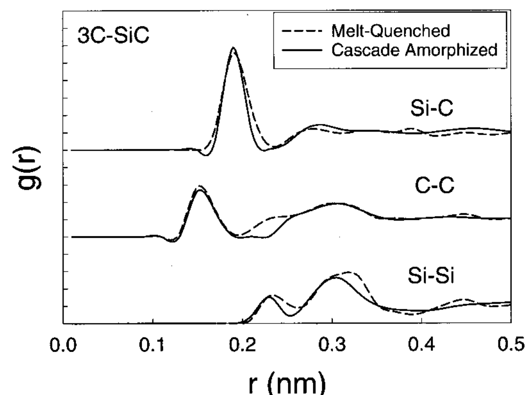

FIG. 6. Calculated pair correlation function g for cascade-amorphized SiC, together with the reference melt-quenched SiC sample for comparison. Separate contributions from Si-C, C-C, and Si-Si pairs are shown, respectively.

The bond-length distribution for amorphous SiC and sample is compared in Fig. 7, where two curves show very similar behavior. The peak positions are consistent with those of the pair-correlation distribution revealed in Fig. 6. Although a large peak appears at the first-neighbor distance of SiC, the distribution is much wider than that in an ordered SiC, and the bond length varies from 0.17 to 0.22 nm, indicating large distortion of the microstructure. Figure 8 shows the bond-angle distribution function for the CA-SiC obtained by damage accumulation, together with the MQ-SiC for comparison. The number of atoms for the tetrahedral bond angle is slightly different for the two curves, but the distribution structure is very similar, suggesting that both CA-SiC and MQ-SiC samples share the same degree of disorder and twist. It is clear that the bond angle is widely distributed in the range from 60° to 140°, which may be associated with various configurations and bonds formed in amorphous SiC, as described above. These results indicate that the atomic arrangements centered at C or Si atoms form distorted tetrahedral binding, and the long-range order translation of SiC is

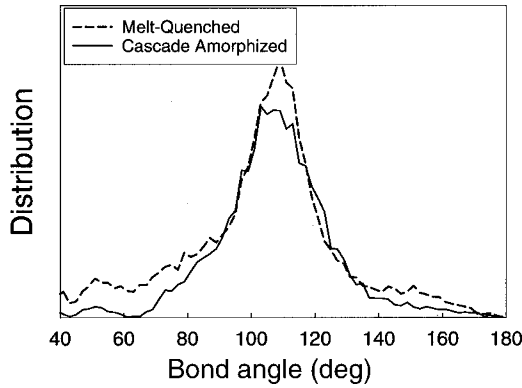

FIG. 8. Comparison between bond-angle distribution functions for amorphous SiC at the end of cascade overlap and the reference amorphous sample.

completely lost when the dose reaches 0.28 MD-dpa. These topological analyses are also consistent with experimental observations, and demonstrate that a *c*-*a* transition occurs during cascade overlap for the dose up to 0.28 MD-dpa. Bolse *et al.*[36] used extended x-ray-absorption fine structure to detect the amorphous structure of SiC and observed a large angle distortion and a number of homonuclear bonds in amorphous SiC under ion irradiation up to the fully amorphous state and higher.

The total and partial coordination numbers for the CA-SiC, which quantifies the atomic distribution and arrangement of each atom, are calculated by integrating the coordination number within the first peak before the first minimum in the total pair-correlation function. The average coordination numbers are listed in Table I, along with those for perfect crystal and the MQ-SiC sample for comparison. Although CA-SiC and MQ-SiC samples are attained by two completely different methods (i.e., irradiation-induced amorphization and melting-quenching process) the total and partial coordination numbers n_t are very similar with values of 3.88 and 3.57 for the CA-SiC and MQ-SiC samples, respectively. The calculated partial coordination number of C n_{CC} is 0.98 and 1.09, which, together with the results for n_{CSi} (2.96 and 2.78), give a total C coordination number of 3.84 and 3.87 for the CA-SiC and MQ-SiC samples, respectively. The small partial coordination number of C is due to the formation of C π-binding in SiC, as in π-bonded graphite. It

TABLE I. Total and partial coordination numbers for perfect crystal, MD melt-quenched, (MD-MQ) amorphous sample, and cascade amorphized (AC) SiC generated by defect accumulation.

Coord. No.	Crystal	MD-MQ sample	CA-SiC
n	4.00	3.57	3.88
n_{C}	4.00	3.87	3.84
n_{CC}	0.00	1.09	0.98
n_{CSi}	4.00	2.78	2.96
n_{Si}	4.00	3.26	3.92
n_{SiSi}	0.00	0.48	0.96
n_{SiC}	4.00	2.78	2.96

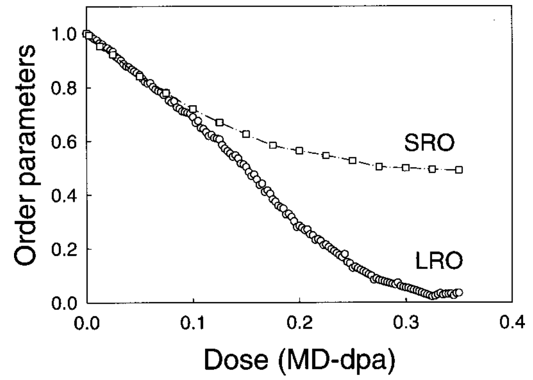

FIG. 9. The variation of Bragg-Willams long-range order parameter S and short-range order parameter η as a function of dose during cascade overlap and defect accumulation for SiC. Note that at the *c*-*a* transition long-range order is almost completely lost; whereas short-range order saturates at about 0.49.

is found that about 25–30 % of bonds formed by C atoms are homonuclear for irradiation-induced amorphous SiC. Finocchi *et al.*[35] employed *ab initio* molecular dynamics to examine the amorphous structure of SiC, and found that the total coordination number of C is smaller than 4.0 in amorphous SiC. The present results are in good agreement with their calculations.

V. ORDER PARAMETERS

The damage states and microstructure changes during cascade overlap can be characterized using long-range order (LRO) and short-range order (SRO) parameters. These parameters provide direct evidence of ordering and disordering of alloys under irradiation,[37] and can be also measured from experiments, such that a full comparison can be made between simulations and experiments. The LRO parameter refers to the degree to which the different sites are occupied by the different types of atoms, and is determined by the arrangement of atoms over the entire crystal. The Bragg-William LRO parameter S is given by the equation[38]

$$S = 1 - \frac{2N_{AB}}{N_A}, \quad (2)$$

where N_{AB} is the number of B atoms associated with A sites and N_A is the total number of A atoms in the crystal. The condition $S=1$ describes the completely ordered state of SiC, whereas $S=0$ expresses the completely disordered state associated with random occupancy of sites. The LRO parameter is shown in Fig. 9 as a function of dose during cascade overlap in SiC. Within the computational error, the LRO parameter decreases steadily with increasing dose, as expected. The reduction is slow at low dose level, which may be associated with the production of point defects and the nucleation of small clusters during the initial stage of damage production and prior to significant cascade overlap, while a rapid decrease appears at doses between 0.05 and 0.25 MD-dpa, which may be related to the enhanced defect production due to cascade overlap, as described in Sec. III. The LRO param-

eter is almost zero when a *c-a* transition occurs, indicating that the long-range order is completely lost in the CA-SiC.

Although the radiation-induced rearrangement of C and Si atoms in SiC can give rise to a reduction of the LRO, the parameter S refers only to the degree of order with regard to the lattice site, but not with respect to atoms themselves. The short-range parameter η characterizes the local arrangement of atoms, and thus, describes the degree of chemical state. It is possible that the degree of long-range order is equal to zero, and simultaneously almost complete short-range order exists in the nonequilibrium states of an alloy. The SRO parameter is defined in its usual manner proposed by Gehlen and Cohen,[39] and given by

$$\eta = \frac{N_{\text{Si-C}}}{2} - 1, \tag{3}$$

where $N_{\text{Si-C}}$ is the number of nearest-neighbor Si atoms to a C atom. $N_{\text{SiC}}=4$ represents complete SRO ($\eta=1$) with the tetrahedral binding of SiC, while $N_{\text{SiC}}=2$ describes the random distribution of atoms ($\eta=0$). By accounting for the neighbor atoms lying within a distance of $0.57a_0$ (a_0 is the lattice parameter of 3C-SiC) of each Si or C and averaging over all atoms in the MD cell, this parameter has been calculated, and is also plotted in Fig. 9 as a function of dose. The distance of $0.57a_0$ is halfway between the first- and second-neighbor space in a perfect SiC. It can be seen that the SRO parameter decreases with increasing dose, but saturates at about 0.49 after a *c-a* transition occurs. Although the long-range order is completely lost in the CA-SiC, the short-range order partially remains, which suggests the existence of some residual tetrahedral network. In an MD study of amorphization due to defect accumulation in SiC irradiated with low energy of 100 eV, the SRO parameter for completely amorphous SiC was found to be about 0.45.[23] In another study,[38] it was found the Au recoils in SiC can produce a large amorphous domain that has a SRO value of 0.42. The good agreement between the present result and previous simulations confirms that the CA-SiC retains a certain degree of local order and a partial correlated tetrahedral network.

VI. DISCUSSION

The purpose of the present simulations was to investigate damage accumulation due to cascade overlap and the mechanisms of amorphization in SiC. It has been shown quantitatively in Figs. 2 and 3, how Frenkel pairs, antisite defects and defect clusters are accumulated as a function of dose. In general, the homogeneous formation of small clusters at low dose and their coalescence at higher dose play a significant role in the *c-a* transition of SiC, resulting in homogeneous amorphization. These clusters have very low mobility and generate considerable strain in crystal, which give rise to the formation of amorphous domains during cascade overlap. The formation of larger clusters or amorphous domains is a defect-stimulated or cascade-induced process. The overlapping of cascades causes or stimulates the growth of clusters from high local defect concentrations and small cluster formation, such that nearby clusters grow and coalesce to form larger clusters or amorphous domains.

Irradiation of SiC with 3.6 MeV Fe^{2+} ions at 300 K to a fluence of 1.4×10^{18} Fe^{2+}/m^2 (0.08 dpa at damage peak) generates small visible defect clusters throughout the irradiation region,[6] but no measurable amorphization. Partial and complete amorphizations were observed at higher dose, 0.2 and 0.4 dpa, respectively. Silicon carbide irradiated with 0.8 MeV He^+ ions to a fluence of 4.7×10^{21} ions/m^2 ($\sim$1.3 dpa at damage peak) showed that complete amorphization occurred in regions with damage levels exceeding 0.8 dpa,[6] but cross-sectional TEM images indicate that the regions adjacent to the amorphous band, with a lower dose level, contained a high density of small defect clusters. These clusters could not be identified as dislocation loops (i.e., two-dimensional clusters), suggesting that these features may be three-dimensional clusters of point defects. By studying the dechanneling cross section as a function of the energy of the analyzing He^+ ions for a SiC layer implanted with 1×10^{14} Xe^+/cm^2 and annealed to 1253 K, Fohl *et al.*[40] have concluded that the irradiated layer contains point defects or small clusters. The similar result was found for light ions.[41] All these experimental observations are consistent with the MD simulation results reported here.

The analysis of defect accumulation, long-range and short-range ordered parameters, as shown in Figs. 3, 4, and 9, suggests that the dose for complete amorphization in SiC is about 0.28 MD-dpa, in agreement with the experimental value under relatively similar irradiation conditions. It should be noted that the experimental amorphization dose is normally obtained by calculating displacement dose using the SRIM code.[26] Thus, the comparison between the present result and experimental value may involve some degree of uncertainty. Numerous studies have been conducted to obtain the threshold dose for complete amorphization SiC under irradiation with ions[6–8,13] and electrons.[10,11] It is generally accepted that the dose for complete amorphization of SiC is between 0.2 and 0.3 dpa for ions and about 1.0 dpa for electrons at low temperatures. Computer simulations of defect accumulation in SiC irradiated with recoil energy of 100 eV by Malerba and Perlado[23] have suggested that the dose for complete amorphization is about 0.94 dpa, which compares well with the value of $\sim$1.0 dpa calculated by Weber *et al.*[8] for experimental electron-irradiation results.[10,11] It is well known that low-energy recoils primarily generate point defects and therefore, should be representative of the average PKA energy spectrum under 2 MeV electron irradiation. However, the very small production of antisite defects of Malerba and Perlado[22] leads them to conclude that the driving force for the c-a transition is only due to the accumulation of Frenkel pairs, which may accurately describe the damage accumulation under electron irradiation. However, the low-energy simulations are in contrast to the present simulations and experimental heavy-ion irradiation.[8,13] On the basis of a high-resolution electron microscopy study of electron-irradiation-induced amorphization in SiC, Inui *et al.*[10] have indicated that electron irradiation can produce antisite defects in SiC, and the accumulation of antisite defects will take place under continued irradiation. It is ob-

served that there are some local regions where a critical concentration will first be reached, above which the crystalline state becomes energetically unstable with respect to the amorphous state, and these regions will preferentially undergo a c-a transition. Weber *et al.*[8,13] noted that there is an apparent discrepancy between the threshold dose and critical temperature for amorphization of SiC irradiated with various ions and electrons, implying that the displacement cascades associated with heavy-ion irradiation may allow amorphization to occur at lower doses and up to higher temperature than would normally be possible with point defect accumulation effects alone. Using Raman spectroscopy, Bolse[42] found that broad bands are visible at the critical threshold fluence for amorphization of SiC irradiated with Na^+, and these bands are shifted slightly towards the position of the crystalline peaks as compared to the high fluence spectra, which indicates the possible generation of antisite defects. These antisite defects would increase the structural freedom, as suggested by Hobbs *et al.*[33]

The topological features of the CA-SiC, such as pair-correlation function, bond-length and bond-angle distribution, are very similar to those for the MQ-SiC sample, considering the completely different procedures followed in either case. These results clearly indicate that various bonds could exist in amorphous SiC, particularly the formation of C-C and Si-Si bonds, but a certain number of Si-C bonds still remains, which implies that disordering of SiC does not lead to a fully connected disordered tetrahedral network. After high fluence irradiation with 4.3×10^{14} Na^+/cm^2 at a temperature of 77 K, Bolse[42] found that there were three broad bands in the Raman spectra, of which two of them could be attributed to C-C and Si-Si bonds. The formation of these bonds was also shown in the x-ray absorption fine-structure spectroscopy (EXAFS) data in addition to the remaining Si-C bonds. The topological features of the present simulations are in good agreement with these experimental observations, and consistent with the molecular dynamics simulations of amorphous SiC quenched from liquid by Finocchi *et al.*[35] who found a complicated disordered structure with sp^2-bonded C chains, surrounded by sp^3-type tetrahedral Si-Si and Si-C networks.

The damage accumulation in SiC involves not only long-range disorder, but also short-range chemical disorder. The Bragg-William LRO parameter and SRO parameter proposed by Gehlen and Cohen[39] have been calculated to describe disordering of SiC during cascade overlap, and it is found that both parameters decrease with increasing dose, as shown in Figs. 9. After a c-a transition occurs, the LRO parameter is completely lost, but the final value of 0.49 for the SRO parameter suggests that partial short-range order remains, which may imply an arrangement of Si-C tetrahedral network in amorphous SiC similar to the crystalline state. Using x-ray absorption fine-structure spectroscopy, Bolse *et al.*[36] measured the degree of long-range and chemical disorders in SiC irradiated with various fluence of 50 keV Na^+ ions at 77 K. The pseudoradial distribution function of the atoms around the Si atom has shown that the irradiation at low dose results in a decrease in the intensity of the Si peaks. The larger radial distance is stronger the effect, which corresponds to the continuous destruction of the long-range order of SiC. After high fluence irradiation with 5.3×10^{14} Na^+/cm^2, the long-range order was observed to be completely lost by means of channeling, but the peak of NNN-Si shell in the x-ray spectroscopy is still visible, indicating that a correlated tetrahedral network exists. A similar observation has been reported by Wendler *et al.*[43] in SiC irradiated with B^+ ions at above room temperature. Only after application of much higher fluences than that for complete amorphization in SiC is a large fraction of the Si-C tetrahedra network destroyed, and hence, the chemical short-range order is removed. Both simulations and experimental observations show that, in spite of observed loss of the overall long-range order in amorphous SiC, the local tetrahedral structure is found to be less disordered compared to the other materials.[22]

VII. SUMMARY

A large number of cascades (140) have been simulated to study cascade overlap, damage accumulation and amorphization using molecular dynamics method in SiC. Single interstitials, monovacancies, antisite defects and small clusters are generated at low dose level, and the homogeneous nucleation of these small clusters corresponds to the experimental observations of homogeneouslike amorphization of SiC under Si^+ and Ar^+ irradiation. The defect stimulated growth and coalescence of clusters to form amorphous domains plays an important role in irradiation-induced amorphization of SiC, and the increase in Frenkel defects and antisite defects with increasing dose suggests that the driving force for c-a transition is due to the accumulation of both Frenkel pairs and antiste defects. The increase in atomic mixing with increasing dose is linear even after a c-a transition, which corresponds to a large atomic rearrangement taking place without further creating defects. The larger mixing efficiency of C atoms indicates more contribution of C atoms to atomic rearrangement during cascade overlap. The pair correlation function, bong-length and bond-angle distributions of irradiated SiC are in excellent agreement to the MD melt-quenched amorphous state. The dose for complete amorphization has been determined to be 0.28 MD-dpa, which is in qualitative agreement with experimental measurements for relatively similar irradiation conditions. Both long-range and short-range order parameters decrease with increasing dose, but the short-range order parameter remains a saturation value of 0.49 after a c-a transition. These results, in conjunction with experimental studies, suggest that there is a certain degree of atomic arrangements of Si-C tetrahedral network similar to the crystalline state in amorphous SiC, even if long-range order is completely lost.

ACKNOWLEDGMENTS

This research was supported by the Division of Materials Science and Engineering, Office of Basic Energy Sciences, U.S. Department of Energy under Contract No. DE-AC06-76RLO 1830.

*Email address: fei.gao@pnl.gov

[1] M. A. Capano and R. J. Trew, MRS Bull. **22**, 19 (1997).
[2] W. Wesch, Nucl. Instrum. Methods Phys. Res. B **116**, 305 (1996).
[3] L. Giancarli, J. P. Bonal, A. Caso, G. Le Marois, N. B. Morley, and J. F. Salavy, Fusion Eng. Des. **41**, 165 (1998).
[4] R. A. Verrall, M. D. Vlajic, and V. D. Krstic, J. Nucl. Mater. **274**, 54 (1999).
[5] B. G. Kim, Y. Choi, J. W. Lee, D. S. Sohn, and G. M. Kim, J. Nucl. Mater. **281**, 163 (2000).
[6] S. J. Zinkle and L. L. Snead, Nucl. Instrum. Methods Phys. Res. B **116**, 92 (1996).
[7] E. Wendler, A. Helt, and W. Wesch, Nucl. Instrum. Methods Phys. Res. B **141**, 105 (1998).
[8] W. J. Weber, N. Yu, L. M. Wang, and N. J. Hess, Mater. Sci. Eng., A **253**, 62 (1998).
[9] W. J. Weber, Nucl. Instrum. Methods Phys. Res. B **166/167**, 98 (2000).
[10] H. Inui, H. Mori, and H. Fujita, Philos. Mag. B **61**, 107 (1990).
[11] H. Inui, H. Mori, and T. Sakata, Philos. Mag. B **66**, 737 (1992).
[12] L. L. Snead and J. C. Hay, J. Nucl. Mater. **273**, 213 (1999).
[13] W. J. Weber, N. Yu, and L. M. Wang, J. Nucl. Mater. **253**, 53 (1998).
[14] W. J. Weber, W. Jiang, S. Thevuthasan, and D. E. McCready, in *Microstructural Processes in Infrared Materials*, edited by S. J. Zinkle *et al.*, MRS Symposia Proceedings No. 540 (Materials Research Society, Pittsburgh, 1999), p. 159.
[15] D. J. Bacon and T. Diaz de la Rubia, J. Nucl. Mater. **216**, 275 (1994).
[16] D. J. Bacon, F. Gao, and Yu. N. Osetsky, J. Nucl. Mater. **276**, 1 (2000).
[17] R. Devanathan, W. J. Weber, and T. Diaz de la Rubia, Nucl. Instrum. Methods Phys. Res. B **141**, 118 (1998).
[18] J. P. Crocombette and D. Ghaleb, J. Nucl. Mater. **295**, 167 (2001).
[19] J. M. Perlado, L. Malerba, A. Sanchez Rubio, and T. Diaz de la Rubia, J. Nucl. Mater. **276**, 235 (2000).
[20] F. Gao and W. J. Weber, Phys. Rev. B **63**, 054101 (2000).
[21] F. Gao, W. J. Weber, and R. Devanathan, Nucl. Instrum. Methods Phys. Res. B **180**, 177 (2001).
[22] W. J. Weber, R. C. Ewing, C. R. A. Catlow, T. Diaz de la Rubia, L. W. Hobbs, C. Kinoshita, Hj. Matzke, A. T. Motta, M. Nastasi, E. K. H. Salje, E. R. Vance, and S. J. Zinkle, J. Mater. Res. **13**, 1434 (1998).
[23] L. Malerba and J. M. Perlado, J. Nucl. Mater. **289**, 57 (2001).
[24] R. Devanathan, W. J. Weber, and F. Gao, J. Appl. Phys. **90**, 2303 (2001).
[25] F. Gao and W. J. Weber (unpublished).
[26] J. F. Ziegler, J. P. Biersack, and U. Littmark, *The Stopping and Range of Ions in Solids* (Pergamon, Oxford, 1985).
[27] R. Devanathan and W. J. Weber, J. Nucl. Mater. **278**, 258 (2000).
[28] F. Gao, E. J. Bylaska, W. J. Weber, and L. R. Corrales, Nucl. Instrum. Methods Phys. Res. B **180**, 286 (2001).
[29] W. Jiang, W. J. Weber, S. Thevuthasan, and D. E. McCready, Nucl. Instrum. Methods Phys. Res. B **143**, 333 (1998).
[30] W. J. Weber, W. Jiang, and S. Thevuthasan, Nucl. Instrum. Methods Phys. Res. B **175–177**, 26 (2001).
[31] X. Yuan and L. W. Hobbs, Nucl. Instrum. Methods Phys. Res. B **191**, 74 (2002).
[32] W. J. Jiang and W. J. Weber, Phys. Rev. B **64**, 125206 (2001).
[33] L. W. Hobbs, A. N. Sreeram, C. E. Jesurum, and B. A. Berger, Nucl. Instrum. Methods Phys. Res. B **116**, 18 (1996).
[34] M. A. Petrich, K. K. Gleason, and J. A. Reimer, Phys. Rev. B **36**, 9722 (1987).
[35] F. Finocchi, G. Galli, M. Parrinello, and C. M. Bertoni, Phys. Rev. Lett. **68**, 3044 (1992).
[36] W. Bolse, J. Conrad, F. Harbsmeier, M. Borowski, and T. Rodle, in *Complex Fluids*, edited by D. Weitz *et al.*, MRS Symposia Proceedings No. 248 (Materials Research Society, Pittsburgh, 1997), p. 319.
[37] M. L. Jenkins and M. Wilkens, Philos. Mag. **34**, 1155 (1976).
[38] F. Gao and W. J. Weber, J. Appl. Phys. **89**, 4275 (2001).
[39] P. C. Gehlen and J. B. Cohen, Phys. Rev. A **139**, 844 (1965).
[40] A. Fohl, R. M. Emrick, and H. D. Carstanjen, Nucl. Instrum. Methods Phys. Res. B **65**, 185 (1992).
[41] C. Calcagno, M. G. Grimaldi, and P. Musumeci, J. Mater. Res. **12**, 1727 (1997).
[42] W. Bolse, Nucl. Instrum. Methods Phys. Res. B **148**, 83 (1999).
[43] E. Wendler, A. Heft, U. Zammit, E. Glaser, M. Marinelli, and W. Wesch, Nucl. Instrum. Methods Phys. Res. B **116**, 398 (1996).